Mathematical modeling and biochemical analysis support partially ordered CaM-MLCK binding

Melissa JS MacEwen[1], Domnita-Valeria Rusnac[1], Henok Ermias[1], Joseph P Dexter[2*], Yasemin Sancak[1*]

[1]Department of Pharmacology, University of Washington, Seattle, WA, USA.
[2]Data Science Initiative and Department of Human Evolutionary Biology, Harvard University, Cambridge, MA, USA.

*Co-corresponding authors: jdexter@fas.harvard.edu, sancak@uw.edu

Running title

Modeling, biochemistry support partially ordered CaM-MLCK binding

Keywords

Calmodulin, mathematical modeling, FRET, calcium signaling, excitation-contraction coupling, myosin light chain kinase

Abstract

Activation of myosin light-chain kinase (MLCK) by calcium ions (Ca^{2+}) and calmodulin (CaM) plays an important role in smooth muscle contraction. Despite extensive biochemical analysis of this system, aspects of the mechanism of activation remain controversial, and competing theoretical models have been proposed for the binding of Ca^{2+} and CaM to MLCK. The models are analytically solvable for an equilibrium steady state and give rise to distinct predictions that hold regardless of the numerical values assigned to parameters. These predictions form the basis of a recently proposed, multi-part experimental strategy for model discrimination. Here we implement this strategy by measuring CaM-MLCK binding using an *in vitro* FRET system. This system quantifies the binding of either wild-type or mutant CaM with defective EF-hand domains to a FRET reporter that uses a fragment of MLCK protein as a proxy for the full protein. Interpretation of binding data in light of the mathematical models suggests a partially ordered mechanism for binding of CaM to MLCK.

INTRODUCTION

Calmodulin (CaM) is a calcium-binding protein found ubiquitously in the cytosol of eukaryotic cells. CaM contains two globular domains joined by a flexible linker. The N-terminal and C-terminal domains each have a pair of EF-hand motifs and are each capable of binding two calcium ions (Ca^{2+}) (1). CaM acts as a regulator or effector in numerous cellular processes, ranging from muscle contraction to glycogen metabolism and synaptic plasticity (2-4). The Ca^{2+}-mediated binding of CaM and either smooth muscle myosin light chain kinase or nonmuscle myosin light chain kinase (henceforth collectively referred to as "MLCK") is central to functions such as vascular smooth muscle contraction and cell motility. CaM-MLCK binding takes place as follows: Ca^{2+} enters the cytosol and binds to the four Ca^{2+} binding sites of CaM, leading to a dramatic change in CaM protein conformation (5). CaM then binds to the CaM-binding domain of MLCK, triggering a conformational change in MLCK that activates the kinase by displacing an autoinhibitory sequence from the kinase's catalytic domain (6,7). Finally, activated MLCK phosphorylates the 20-kDa regulatory light chains of myosin II, resulting in contraction caused by myosin cross-bridges moving along actin filaments.

Multiple formal models have been proposed for the activation of MLCK by Ca^{2+} and CaM (8-11). Given the cooperative nature of Ca^{2+} binding at both the C- and N-terminus of CaM, each of these models treats CaM as having two Ca^{2+} binding sites. The model of Brown *et al*. (8) and Fajmut, Brumen *et al*. (9) makes no further assumptions, giving rise to an eight-state reaction network in which MLCK may bind to CaM before or after Ca^{2+} ("Model 1" in **Fig. 1A**). Other previously proposed models are truncations of this network, in which the binding of Ca^{2+} and MLCK is either partially (10) or fully (11) ordered ("Model 2" and "Model 3" in **Fig. 1A**, respectively). Accordingly, Model 1 corresponds to a fully random binding mechanism (Ca^{2+} and MLCK can bind to CaM in any order), Model 2 to a partially ordered mechanism (MLCK can bind to CaM after Ca^{2+} is bound at the C-terminus), and Model 3 to a fully ordered mechanism (MLCK can bind to CaM only after Ca^{2+} is bound at both the C-terminus and N-terminus).

In recent work, Dexter *et al*. showed that this class of models is analytically solvable for a CaM/MLCK system at both thermodynamic equilibrium and steady state, and that each model predicts distinct steady-state behavior in certain Ca^{2+} concentration regimes (12). Importantly, these predictions hold regardless of the numerical values assigned to the model parameters (i.e.,

the equilibrium constants in **Fig. 1A**), allowing us to develop a strategy for model discrimination that does not require extensive parameter estimation.

Our experimental approach involves quantifying the fraction of MLCK bound to CaM under different [Ca^{2+}] in which CaM is in large molar excess over MLCK. We implement a multistep strategy for model discrimination, in which we first compare Model 1 to Models 2 and 3 and then compare Model 3 to Models 1 and 2. During the first step, MLCK-CaM binding at zero [Ca^{2+}] is determined, as Model 1, but not Models 2 and 3, predicts binding under these conditions. In the second step, binding of MLCK to a CaM mutant unable to bind Ca^{2+} at its N-terminus is measured at high [Ca^{2+}]; Models 1 and 2, but not Model 3, predict binding between MLCK and this mutant CaM. Finally, we use a CaM mutant with impaired C-terminal Ca^{2+} binding to evaluate additional predictions of Model 2.

To test the predictions of the models experimentally, we use an established fluorescence resonance energy transfer (FRET) system that has been deployed to characterize CaM- and Ca^{2+}-dependent activation of MCLK both *in vivo* and *in vitro* (13-18). Notably, in HEK 293T lysates phosphorylation of myosin has been shown to track changes in FRET signal, such that the FRET reporter (FR) can quantify MLCK activation (19). We measure MLCK-CaM binding across a wide range of [Ca^{2+}] for wild-type CaM (CaM^{WT}) and three different CaM mutants: CaM with its N-terminal EF-hands mutated (D21A and D57A mutations, $CaM^{21A,57A}$; **Fig. 1B**), CaM with its C-terminal EF-hands mutated (D94A and D130A mutations, $CaM^{94A,130A}$; **Fig. 1C**) and CaM with all of its EF-hands mutated (D21A, D57A, D94A, D130A,$CaM^{21A,57A,94A,130A}$). The use of these four different forms of CaM is central to our model discrimination strategy, as it enables us to evaluate each key prediction of the mathematical models. Our binding measurements falsify key predictions of both Model 1 (random binding) and Model 3 (fully ordered binding) but are consistent with multiple distinct predictions of Model 2, which strongly suggests that CaM-MLCK binding follows a partially ordered mechanism.

RESULTS

In the FRET system, the FR is composed of a YFP and ECFP FRET pair, which are linked by the CaM-binding domain of smooth muscle MLCK(19). FR thus acts as a proxy for the full MLCK protein in our experiments. Binding of CaM to FR interferes with FRET, enabling quantification of MCLK-CaM binding as the ratio of YFP and ECFP emission (F480/F353) after excitation at 430nm

(**Fig. 2A**). FLAG-tagged FR was purified from HEK 293T cells after transient transfection, and His-tagged CaM^{WT} and CaM mutants ($CaM^{21A,57A}$, $CaM^{94A,130A}$, and $CaM^{21A,57A,94A,130A}$) were purified after bacterial expression. Gel electrophoresis and SYPRO™ Ruby staining of purified proteins (**Fig. 2B**), as well as mass spectrometry analysis (**Fig. S1**), established that the protein preparations were free of major contaminants. In addition, we observed an expected Ca^{2+}-dependent conformation change and gel mobility shift in CaM^{WT}, $CaM^{21A,57A}$, and $CaM^{94A,130A}$ (**Fig. 2B**) (20). This shift illustrates the Ca^{2+}-binding properties of our different CaM proteins.

The previous theoretical analysis identified a two-part strategy for distinguishing between the three models of CaM-MLCK binding, which is described in detail in Dexter *et al.* (12). The analysis involved deriving algebraic expressions for the fraction of total MLCK (*F*) that is bound to CaM as a function of free [Ca^{2+}] for each of the models; plots of *F* are shown in **Fig. 3** for CaM^{WT} (**A**), $CaM^{21A,57A}$ (**B**), $CaM^{94A,130A}$ (**C**), and $CaM^{21A,57A,94A,130A}$ (**D**), respectively (assuming the reference values for the equilibrium constants compiled by Fajmut, Brumen *et al.* (9) and the concentrations of CaM and MLCK used in our experiments). The model discrimination strategy rests on two predictions that differ between the three models and that hold true regardless of the specific numerical values assigned to the model parameters, such as the equilibrium constants in **Fig. 1**. The first is that only Model 1 predicts non-zero binding of MLCK in zero [Ca^{2+}], with the fraction bound given by the following expression:

$$F_1(0) = \frac{2K_9 CaM_{tot}}{1+K_9(M_{tot}+CaM_{tot})+\sqrt{1+2K_9(CaM_{tot}+M_{tot})+K_9^2(CaM_{tot}-M_{tot})^2}}, \quad (1)$$

where CaM_{tot} and $MLCK_{tot}$ denote total CaM and total MLCK, respectively. The second is that only Model 3 predicts zero binding of MLCK to a CaM mutant with nonfunctional N-terminal EF hands, such as $CaM^{21A,57A}$, at any free [Ca^{2+}]. In contrast, both Models 1 and 2 predict non-zero binding, with the fraction in the high-[Ca^{2+}] limit given by

$$\lim_{[Ca^{2+}]\to\infty} F_1{}^* = \lim_{[Ca^{2+}]\to\infty} F_2{}^* = \frac{2K_4 CaM_{tot}}{1+K_4(CaM_{tot}+M_{tot})+\sqrt{1+2K_4(CaM_{tot}+M_{tot})+K_4^2(CaM_{tot}-M_{tot})^2}}. \quad (2)$$

To test these predictions experimentally, we used a plate reader to measure CaM-FR binding as a function of free [Ca^{2+}] with a 30-fold molar excess CaM^{WT}, $CaM^{21A,57A}$, $CaM^{94A,130A}$, or $CaM^{21A,57A,94A,130A}$ relative to FR. [CaM] was 673 nM (13 ng/µl), and [FR] was 22.9 nM (1.3 µg/µl).

After collecting Ex430/ Em480 and Ex430/Em535 data from different FR-CaM pairs (**Fig. S3**), we divided each [Ex430/Em480] fluorescence intensity value by its corresponding [Ex430/Em535] value to yield a ratio, which is plotted in **Fig. 3**. We confirmed the presence of excess CaM compared to FR, and equal protein amount across experiments, by SDS-PAGE and SYPRO™ Ruby staining of the samples after FRET measurement (**Fig. S2**).

For the first model discrimination test, we compared the FRET signal with CaM^{WT} and FR with baseline in zero and low [Ca^{2+}]. Contrary to the prediction of Model 1, we find no evidence that the signal in zero [Ca^{2+}], or the area under the binding curve for 0 μM ≤ [Ca^{2+}] ≤ 0.038 μM, is higher than baseline (p = 0.994 and p = 0.995, respectively, by a one-tailed Mann-Whitney U test). For the second test, we compared the FRET signal with $CaM^{21A,57A}$ and FR in high Ca^{2+}. We found that FRET in the maximum concentration used (39 μM [Ca^{2+}]) is significantly higher than baseline ($p = 2.83*10^{-6}$ by a one-tailed Mann-Whitney U test), as is the area under the complete binding curve ($p = 2.83*10^{-6}$ by a one-tailed Mann-Whitney U test). These observations are sufficient to falsify Model 3, which predicts zero binding of MLCK to any CaM mutant with impaired N-terminal Ca^{2+} binding. As such, only the predictions of Model 2 are consistent with the full set of experimental results. As an additional test of Model 2, we examined binding of $CaM^{94A,130A}$ in high [Ca^{2+}]; consistent with the predictions of the model, we found no significant difference over baseline for the FRET signal in 39 μM [Ca^{2+}] or for the area under the complete binding curve (p = 0.345 and p = 0.294, respectively, by a one-tailed Mann-Whitney U test).

After completing the model discrimination analysis, we performed a series of control experiments to test whether the presence of CaM altered FR properties other than FRET interference and whether free [Ca^{2+}] was altered as a result of CaM storage buffer addition during FRET assays. First, we collected 460 nm - 700 mm emission spectra of the FR with Ex430, which showed two peaks at ~ Em480 and ~Em535 (**Fig. S4**). FR did not show any changes in FRET as a function of [Ca^{2+}] (**Fig. S4**). CaM^{WT} and $CaM^{21A,57A}$ caused an increase at ~Em430 and a decrease at ~Em535 in the presence of Ca^{2+} only; $CaM^{94A,130A}$ did not change the spectra noticeably at any wavelength, with or without Ca^{2+} (**Fig. S4**). To determine the effects of buffer addition on free [Ca^{2+}], we measured the fluorescence intensity of two Ca^{2+} indicator dyes with different Ca^{2+} affinities (Fluo-4 and Calcium Green), before and after addition of CaM storage buffer (largest volume used in our experiments, 1.3 μl per assay). We did not observe a significant change in reporter fluorescence intensity after CaM storage buffer addition, which suggests that any

changes to free [Ca^{2+}] are smaller than can be detected reliably with Fluo-4, a dye that has a very high Ca^{2+} affinity (17 nM) **(Fig. S5)** (*p* =0.23-0.99 by a two-tailed Mann-Whitney *U* test).

In our FRET-based binding experiments, we observed binding only between FR-CaM^{WT} and FR-$CaM^{21A,57A}$. To confirm that these interactions are specific and Ca^{2+}-dependent, we performed several *in vitro* binding assays. When immunoprecipitated FLAG-FR was incubated in 50 µl of buffer with 505 nM CaM^{WT} (approximately 20 ng/µl), the fraction of CaM^{WT} bound to FR increased proportionally with free [Ca^{2+}]. At 39 µM [Ca^{2+}], almost all of the CaM^{WT} input was bound to the FR (**Fig. 4A**). When the same experiment was repeated using $CaM^{21A,57A}$, the majority of $CaM^{21A,57A}$ bound to FR at 39 µM Ca^{2+} (**Fig. 4B**). These results suggest that the purified CaM proteins are functional and bind to Ca^{2+} and the FR, and that there is negligible non-specific binding between the FR and the purified CaM proteins.

We did not observe any changes in Em480/Em535 ratio when FR was incubated with $CaM^{94A,130A}$ or $CaM^{21A,57A,94A,130A}$. To investigate the possibility that $CaM^{94A,130A}$ or $CaM^{21A,57A,94A,130A}$ might bind to the FR but fail to interfere with FRET, we used a Bio-Layer Interferometry (BLI) assay as an orthogonal method to measure binding between FR and CaM (**Fig. 5**). Binding detection in the BLI assay is independent of FRET measurement, which enabled us to decouple binding and FRET interference. The BLI assay showed no binding between FR and CaM^{WT} at zero [Ca^{2+}], robust binding between FR and CaM^{WT} at high [Ca^{2+}], and no detectable binding between FR and $CaM^{94A,130A}$ or $CaM^{21A,57A,94A,130A}$ at zero or high [Ca^{2+}] (**Fig. 5**).

The effectiveness of our model discrimination strategy also depends on the intrinsic sensitivity of the FRET assay. To test if our assay can detect small changes in binding, which is necessary for many of the comparisons involved in the analysis, we measured FRET at 39 µM [Ca^{2+}] with different FR:CaM ratios. Assuming Model 2 and the reference parameter values from Fajmut, Brumen *et al*. (9), if the FR:CaM molar ratio is increased from 2:1 to 2:1.2, the amount of CaM-bound FR in 39 µM [Ca^{2+}] is predicted to increase by 8.5% (from 46.2% bound to 54.7% bound). When we repeated our FRET based FR:CaM binding assay using these ratios (22.9 nM FR and 11.45 nM or 13.75 nM CaM), we observed a significant increase in F480/F535 **(Fig. S6)** (*p* =0.00029 by a one-tailed Mann-Whitney *U* test), with an 8.7% difference between the two conditions**.** We therefore conclude that, under our experimental conditions, the assay is sensitive enough to detect at least an 9% increase in the fraction of CaM-bound FR.

The predictions of zero MLCK binding in a particular [Ca^{2+}] hold for any set of numerical values assigned to the model parameters (the equilibrium constants K_1...K_{11} in **Fig. 1)**, as shown in Dexter *et al.* (12). For predictions of non-zero binding, however, the magnitude of binding does depend on the choice of parameters. As such, it is theoretically possible that the model could predict a binding fraction that is non-zero but too small to detect experimentally in an important concentration regime. To address this potential concern, we undertook a sensitivity analysis of the two key predictions of non-zero MLCK binding. For numerical calculations with the models, we used the set of reference parameter values compiled by Fajmut, Brumen *et al*. from previous biochemical studies (9). As shown in Eq. 1, the prediction of Model 1 for the fraction of MLCK bound in zero [Ca^{2+}] depends on the value of a single parameter (K_9). Assuming the parameter value selected by Fajmut, Brumen *et al.* (9) based on several prior studies (K_9 = 0.078 μM^{-1}) and the concentrations of CaM^{WT} and FR used in the main experiment, the model predicts 5.2% binding in zero [Ca^{2+}]. As is clear from the structure of Eq. 1, the fraction of MLCK bound in zero [Ca^{2+}] increases with the ratio of total CaM to total MLCK. To confirm our falsification of Model 1, we therefore repeated the binding experiment in zero [Ca^{2+}] with much higher [CaM] (35.65 μM), for which 73.5% binding is predicted with the reference parameter values and 21.7% binding is predicted with K_9 = 0.0078 μM^{-1}. As in the main experiment, the FRET signal did not increase in zero [Ca^{2+}] (**Fig. S7**), providing strong evidence against Model 1 even if previous parameter estimates are incorrect by an order of magnitude (p =0.998 by a one-tailed Mann-Whitney U test). For Model 2 with $CaM^{21A,57A}$ the fraction of MLCK bound depends on the parameters K_4 and K_6 (12). We confirmed the robustness of the key prediction of non-zero binding in 39 μM [Ca^{2+}] by calculating F^* for 200,000 combinations in which values for each of the two parameters were chosen at random from the interval [0.1v, 10v], where v is the reference value from Fajmut, Brumen *et al*. (9). Across the combinations F was never less than 18%; the full distribution is shown in **Fig. S8**.

In sum, our binding measurements using the FR falsify key predictions of both the fully random binding mechanism (Model 1) and the fully ordered binding mechanism (Model 3). Our data instead support Model 2, which predicts partially ordered binding between CaM and MLCK (**Fig. 1**). As predicted by Model 2, we observe zero binding in low [Ca^{2+}] for CaM^{WT} and all mutants, non-zero binding in high [Ca^{2+}] for CaM^{WT}, non-zero binding in high [Ca^{2+}] for N-terminal mutant $CaM^{21A,57A}$, and zero binding in high [Ca^{2+}] for both of our CaM mutants containing mutations in the C-terminus domain ($CaM^{94A,130A}$ and $CaM^{21A,57A,94A,130A}$). Model 2 makes six correct predictions and no incorrect predictions (**Table 1**). Model 1 makes two falsified predictions: non-zero binding

in low [Ca^{2+}] for CaM^{WT}, and non-zero binding in high [Ca^{2+}] for the C-terminus mutant, $CaM^{94A,130A}$. Finally, Model 3 makes one falsified prediction: non-zero binding in high [Ca^{2+}] for the N-terminus mutant, $CaM^{21A,57A}$.

DISCUSSION

In recent work, Dexter *et al.* analyzed a class of previously developed theoretical models of CaM-MLCK binding and proposed a multi-part strategy for distinguishing between them (12). Our primary contribution here is an experimental implementation of this model discrimination strategy, which suggests a partially ordered mechanism for binding. Our analysis sheds new light on a controversy that has persisted for several decades and demonstrates a productive interplay between mathematical modeling and biochemical analysis.

It is important to remember that model discrimination strategies of this kind work by process of elimination. Models can be ruled out when their predictions contradict experimental data, but the failure of some models does not guarantee the correctness of others. We present here evidence sufficient to falsify all but one of the models of CaM-MLCK binding in the literature (**Table 1**). Data collected using wild-type and mutant CaM proteins in three different binding experiments (FRET, BLI and *in vitro* binding) in zero and high [Ca^{2+}] rule out both Model 1 (a fully random binding mechanism in which MLCK may bind to CaM before or after Ca^{2+}) and Model 3 (a fully ordered mechanism in which MLCK can bind to CaM only after Ca^{2+} is bound at both the C-terminus and N-terminus). In addition, we observe no binding of the $CaM^{94A,130A}$ mutant in high [Ca^{2+}]. Taken together, these results strongly support a partially ordered mechanism in which MLCK can bind to CaM after Ca^{2+} is bound at the C-terminus (Model 2).

To investigate MCLK-CaM binding, we utilized a FR system that uses the CaM binding domain of smooth muscle MLCK, rather than the full protein. Prior studies have demonstrated that this reporter accurately reflects the MLCK-CaM binding in a variety of *in vivo* and *in vitro* contexts (13-18). Moreover, our *in vitro* FR-CaM binding FRET assay enabled collection of robust and reproducible data using purified CaM and FR proteins, with minimal risk of interference from endogenous proteins or contaminants. This system is also amenable to complementary, non-FRET-based biochemical techniques to assess FR-CaM binding, which allowed us to confirm the FRET-based binding data we obtained. Despite these strengths, structural studies that compare

FR-CaM and MLCK-CaM binding are needed to conclusively show that FR and full-length MLCK interact with CaM similarly.

It should be noted that mammalian myosin light chain kinases are a group of serine/threonine kinases encoded by at least four genes: *MYLK1*, *MYLK2*, *MYLK3*, and *MYLK4* (21). *MYLK1* has alternative initiation sites that enable expression of at least four protein products including nonmuscle (long isoform) MLCK and smooth muscle (short isoform) MLCK. *MYLK2* encodes an MLCK isoform expressed solely in skeletal muscle, *MYLK3* encodes a cardiac-specific MLCK (MLCK3), and the gene product(s) of *MYLK4* remain largely uncharacterized (20,21). All MLCK proteins, except MLCK4, have a CaM-binding peptide that shows sequence homology to the peptide used in our FR, which is derived from smooth muscle MLCK. As a result, we expect that our findings here can be generalized to other MLCK proteins and their interaction with CaM and Ca^{2+}.

In addition to providing a blueprint for future model discrimination efforts that integrate mathematical and biochemical approaches, our work may also prove useful in a translational or pharmaceutical context, as MLCK and its activation by CaM have been linked to the pathogenesis of human disease. For example, increased organization of the sarcomere, the contractile unit of the striated muscle, is observed during the onset of cardiomyocyte hypertrophy. CaM-activated MLCK has been shown to mediate sarcomere organization induced by a hypertrophic agonist in cultured cardiomyocytes and *in vivo* (22). Fuller characterization of the Ca^{2+}-CaM-MLCK interaction network may therefore prove relevant for future drug discovery efforts.

EXPERIMENTAL PROCEDURES

Cell Culture

- DMEM; Thermo Fisher Scientific, cat. no. 11-965-118
- Glutamax; Fisher Scientific, cat. no. 35-050-061
- PBS; Thermo Fisher Scientific, cat. no. 20012050
- Penicillin/streptomycin solution; VWR cat. no. 45000-652
- Fetal bovine serum; Life Technologies, cat. no. 26140087
- Genlantis MycoScope PCR Detection Kit; VWR cat. no. 10497-508

HEK 293T cells were acquired from the Sabatini Lab at the Whitehead Institute for Biomedical Research. The identity of the cell line was confirmed using STR analysis. Cells were grown in

DMEM supplemented with 1X GlutaMAX and 10% fetal bovine serum. Cells were tested for mycoplasma every 3 months and were confirmed to be free of mycoplasma contamination.

Gel Sample Preparation, Running, and Imaging

Reducing sample buffer, pH 6.8

- SDS; Sigma-Aldrich Cat. no. L4509-1KG
- BME/2-mercaptoethanol; Sigma-Aldrich Cat. no. M3148-25ML
- Glycerol; Sigma-Aldrich Cat. no. G5516-1L
- Tris–HCl: Sigma-Aldrich cat. no. T5941
- Bromophenol Blue; VWR Cat. no. 97061-690

Gel Electrophoresis

- 10X Tris/Glycine Buffer; Boston BioProducts Cat. no. BP-150-4L
- Tris-Glycine 12% Gel, 10-well or 15-well; Bio-Rad Cat. No. 4561043 or 4561046

Gel Imaging

- Methanol; Sigma-Aldrich cat. no. 32213-2.5L
- Acetic Acid; Sigma-Aldrich cat. no. A6283-500ML

Gels were stained with SYPRO® Ruby Protein Gel Stain (# S12000) following manufacturer's instructions and imaged with iBrightCL 1000 on fluorescent protein gel setting.

Expression of MLCK FR via transient transfection

- Transfection reagent; X-treme(GENE) 9, Sigma-Aldrich, cat. no. 6365779001

Day 1: Either 5 million (purification) or 2 million (binding assays) HEK 293T cells were plated on 15 cm or 10 cm plates, respectibely. *Day 2*: 5 µg (purification) or 1.5 µg (binding assays) of MLCK-FLAG FR plasmid was transfected using transfection reagent. *Day 4*: Cells were harvested, and MLCK reporter was either purified (see below, "Purification of FR") or used for CaM-MLCK binding assays.

Purification of FR

Lysis Buffer

- 50 mM HEPES-KOH **(**HEPES, Sigma-Aldrich, # H3375-1KG KOH, Sigma Millipore, # 1050121000)
- 150 mM NaCl, Sigma-Aldrich, # 746398-5KG
- 5 mM Ethylenediaminetetraacetic acid (EDTA): Sigma-Aldrich, # 607-429-00-8
- 1% Triton X-100: Sigma, # X100-1L

- FLAG Peptide Elution Buffer: 50 mM HEPES, 500 mM NaCl, pH 7.4
- Protease Inhibitor Tablets; Complete™, Mini, EDTA-free Protease Inhibitor Cocktail, Sigma-Aldrich cat. no. 5892953001
- Anti-FLAG affinity gel; Sigma-Aldrich, cat. no. A2220-5ML
- 3X FLAG peptide; Sigma-Aldrich cat. no. F4799-4MG
- Chromatography spin column; Bio-Rad cat. no. 7326204

Cells were lysed using lysis buffer supplemented with proteases inhibitors. Lysates were triturated in tubes and then centrifuged at 17000 g for 10 minutes. Cell supernatant was divided into three tubes with 200 µl of anti-FLAG affinity gel slurry (50:50 bead/lysis buffer). These tubes were rocked at 4 °C for 1 hour, and beads were washed three times with lysis buffer. A 22.5-gauge syringe was used to aspirate all remaining liquid from the tubes. FLAG-tagged protein was eluted with 90 µl of elution buffer, and 10 µl of 3XFLAG peptide prepared at 5 mg/mL for 30 minutes at 30 °C. The gel/elution buffer slurry from all three tubes was then pipetted into one spin column and spun at max speed for 5 minutes.

Expression and Purification of Wild-type and Mutant CaM via Bacterial Induction

- Low-salt LB broth: Millipore Sigma, # L3397-1KG
- Isopropyl beta-D-1-thiogalactopyranoside (IPTG): Sigma-Aldrich, # I5502-5G
- HiTrap Q HP anion exchange chromatography column: Cytiva, # 17115301
- Centrifugal protein concentrator, 10K cutoff: Amicon, # UFC8010

Lysis Buffer

- 20 mM Tris-HCl, Sigma-Aldrich cat. no. T5941
- 100 mM NaCl, Sigma-Aldrich, cat. no. 746398-5KG
- 20 mM imidazole, Sigma-Aldrich, cat. no. I5513
- 0.4 mM EGTA, Sigma-Aldrich cat. no. 324626-25GM
- 0.5 mM TCEP, Sigma-Aldrich cat. no. C4706-2G

Elution Buffer

- 20 mM Tris-HCl, Sigma-Aldrich cat. no. T5941
- 100 mM NaCl, Sigma-Aldrich, cat. no. 746398-5KG
- 200 mM imidazole, Sigma-Aldrich, cat. no. I5513
- 0.4 mM EGTA, Sigma-Aldrich cat. no. 324626-25GM
- 0.5 mM TCEP, Sigma-Aldrich cat. no. C4706-2G

Buffer A:

- 100 mM NaCl, Sigma-Aldrich, cat. no. 746398-5KG

- 20 mM Tris-HCl, Sigma-Aldrich cat. no. T5941

Buffer B:

- 1M NaCl, Sigma-Aldrich, cat. no. 746398-5KG
- 20 mM Tris-HCl, Sigma-Aldrich cat. no. T5941

BL21 (DE3) bacteria transformed with a CaM expression vector were grown at 37 ºC, 200 RPM until OD600 reached 0.8-1.0. Cultures were cooled to 18 ºC and supplemented with IPTG to a final concentration of 0.3 mM before incubation at 18 ºC, 200 RPM for 18 hours. Bacteria were pelleted, frozen, and stored at -80 °C until protein purification. Cells were lysed using sonication for 5 minutes at 40% power before being centrifuged at 17,400 RPM for 40 minutes to separate the soluble and insoluble portions of the lysate. The clarified lysate was loaded onto a Ni-NTA gravity column and then washed with 10 column volumes of lysis buffer before elution with 5 column volumes of elution buffer. The eluted protein was loaded manually into a 1 ml anion exchange chromatography column. HPLC was performed using buffers A and B. The HPLC fractions that contained the highest concentrations of protein were collected and concentrated to their final concentrations using a centrifugal filter with a 10 kDa molecular weight cutoff. Stock protein concentrations were as follows: CaM^{WT}: 3.98 µg/µl; $CaM^{21A,57A}$: 4.96 µg/µl; $CaM^{94A,130A}$: 1.36 µg/µl; $CaM^{21A,57A,94A,130A}$: 1.52 µg/µl. Purified protein was aliquoted, flash frozen in a liquid nitrogen dewar, and then stored at -80 °C until use.

<u>Fluorescence Based CaM-FR Binding Assay</u>

- Calcium calibration buffer kit; Invitrogen cat. no. C3008MP
- Microplate reader; BioTek Synergy H1
- Black 96-well plates; Greiner Bio-One cat. no. 655076

For each CaM-FR binding assay condition, 2 µg of CaM (either wild-type or mutant) and 200 ng FR was thoroughly mixed with 150 µl of Ca^{2+} buffer (14 conditions between 0 µM and 39 µM). 150 µl of the resulting mixture was pipetted into 1 well of a 96-well plate (Greiner Bio-One, # 655076). CaM was used at a final concentration of 673 nM (13 ng/µl); FR was used at a final concentration of 22.9 nM (1.3 µg/µl). All protein preps (FR and CaM) were at sufficiently high concentrations that each protein addition added negligible volume; stock protein concentrations were as follows: CaM^{WT}: 3.98 µg/µl; $CaM^{21A,57A}$: 4.96 µg/µl; $CaM^{94A,130A}$: 1.36 µg/µl; $CaM^{21A,57A,94A,130A}$: 1.52 µg/µl; FR: 0.52 µg/µl. Follow-up experiments with Ca^{2+} indicator dyes confirmed that the final [Ca^{2+}] were unaffected by the addition of CaM or FR to the Ca^{2+} buffer (see “CaM and Ca^{2+} Buffer with Ca^{2+} Indicator Dye Assay” below). For functional assay, all 14 Ca^{2+} conditions were tested together, batch-wise. All wells were read at 430, 480

excitation/emission, and then again at 430, 535 excitation/emission using a microplate reader. The [430, 480] read was divided by the [430, 535] read to yield an emission ratio, which was plotted relative to [Ca^{2+}]. A small portion of each prepared Ca^{2+} condition was conserved and prepared with sample buffer, to be loaded onto a gel and stained.

CaM-FR Binding Sensitivity Assays

- Microcon concentrator column, Millipore cat. No. 42407

To test the robustness of the falsification of Model 1 to uncertainty in parameter values, we repeated the binding assay in zero [Ca^{2+}] using 35.65 μM CaM^{WT}. CaM^{WT} was concentrated to a stock concentration of 66.6 μg/μl using a concentrator column so that a comparable volume of protein stock (relative to previous assays) could be used. The "CaM-MLCK-FLAG FR Functional Assay" was then performed as described above, except using 35.65 μM CaM^{WT}.

To determine a lower sensitivity limit for the CaM-FR binding assay, 22.9 nM FR was added to 150 μl of high Ca^{2+} buffer along with either 11.45 or 13.74 nM CaM^{WT}, which resulted in a CaM^{WT}:FR molar ratio of either 1:2 or 1.2:2. 150 μl of the resulting mixture was then read in a plate reader using the program employed by the "Fluorescence Based CaM-FR Binding Assay" (see above) and analyzed accordingly.

CaM-FR Spectral Scanning

- Calcium calibration buffer kit; Invitrogen cat. no. C3008MP
- Microplate reader; BioTek Synergy H1
- Black 96-well plates; Greiner Bio-One cat. no. 655076

CaM and FR were added to either 0 or 39 μM [Ca^{2+}] as per "CaM-MLCK-FLAG FR Functional Assay" above. CaM was used at a final concentration of 673 nM (13 ng/μl); FR was used at a final concentration of 22.9 nM (1.3 μg/μl). Using an excitation wavelength of 430 nm, the wells were read using spectral scanning between wavelengths 460 nm and 700 nm, with an emission step of 10 nm. The fluorescence intensity of each wavelength was then plotted.

CaM-FR *In Vitro* Binding Assay

Assay data was collected under 8 different conditions: immunoprecipitated FR and CaM under 6 different [Ca^{2+}] (0 μM, 0.1 μM, 0.35 μM, 1.35 μM, 3 μM, and 39 μM) and two controls (immunoprecipitated FR alone in 39 μM [Ca^{2+}]; beads with CaM in 39 μM [Ca^{2+}]).

Binding Assay Protocol: Transiently transfected cells were washed once with chilled PBS, and then harvested in 1% Triton buffer using a cell scraper. Cells were triturated to ensure complete lysis, and then were spun down at maximum speed (17,000g) for 10 minutes using a 4 ^{o}C centrifuge. 160 µl bead:glycerol M2 FLAG slurry was prepared for immunoprecipitation by washing three times with 1 ml 1% Triton buffer before being divided evenly between 8 tubes. The cleared lysate from the transiently transfected cells was divided evenly between 7 of the tubes, while cleared lysate from control WT HEK 293T was added to the 8th tube (control lysate). The beads were incubated with the lysate on a rocker at 4 ^{o}C for 45 minutes. After incubation, the two control tubes were washed twice with 200 µl 39 µM [Ca^{2+}], while the tubes for the 6 different Ca^{2+} conditions were each washed with the appropriate Ca^{2+} buffer. 50 µl of the appropriate Ca^{2+} buffer was then added to each experimental tube, while 50 µl of 39 µM Ca^{2+} was added to each control tube. Finally, 0.5 µg of CaM was added to all tubes except the reporter-only condition; final CaM concentration was approximately 505 nM (10 ng/µl). CaM stock was at a sufficiently high concentration to ensure the addition of CaM did not meaningfully alter Ca^{2+} buffer concentration (see "CaM and Ca^{2+} Buffer with Ca^{2+} Indicator Dye Assay below") (**Fig. S5**). All tubes were incubated at room temperature for 15 minutes and were flicked occasionally. Following incubation, the tubes were spun for 1 minute at 1,000 g to pellet the beads. 40 µl of the unbound portion was conserved and prepared with 10 µl 5X reducing sample buffer. The beads for all conditions were then washed with 50 µl of the appropriate Ca^{2+} buffer and all liquid was aspirated from the beads using a syringe to remove residual unbound CaM. The beads were then incubated with 40 µl of FLAG peptide prepared in elution buffer for 30 minutes at 30°C to elute FLAG tagged FR. After elution, the beads were loaded to a spin column and spun for 1 minute at 1000g at room temperature to recover the eluate without the beads. This eluted sample was then boiled with 10 µl 5X reducing sample buffer. Finally, an "input" sample was prepared by adding 0.5 µg of CaM to 40 µl of 39 µM [Ca^{2+}] solution and 10 µl 5X reducing sample buffer.

<u>CaM and Ca^{2+} Buffer with Ca^{2+} Indicator Dye Assay</u>

- Calcium Green 5N, Hexapotassium Salt, Cell Impermeant; Thermo Fisher Scientific, cat. no. C3737
- Fluo-4 Cell Impermeant; Thermo Fisher Scientific, cat. no. F14200
- Microplate reader; BioTek Synergy H1
- Calcium calibration buffer kit; Invitrogen cat. no. C3008MP
- Black 96-well plates; Greiner Bio-One cat. no. 655076

CaM Storage Buffer ("Dummy Buffer")

- 250 mM NaCl, Sigma-Aldrich, cat. no. 746398-5KG
- 20 mM Tris, pH 8, Sigma-Aldrich cat. no. T5941

This assay was performed to confirm that the addition of CaM protein to the Ca^{2+} buffer used for the CaM-FR binding assay did not change the final [Ca^{2+}]. Two "sets" of each of the 14 different Ca^{2+} buffers used for CaM-FR binding assay were prepared, with dye (Calcium Green or Fluo-4) added to a final concentration of 1 μM. For one set of buffers, the buffer in which the CaM proteins was stored was added ("dummy buffer"). The amount of "dummy buffer" added was equal in volume to the maximum volume of CaM added per reaction (ie the C-terminus mutant CaM was the most dilute CaM prep, and approximately 1.5 μl CaM was added to each assay well, so an equivalent amount of "dummy buffer" was used for these experiments). 150 μl of each of these prepared buffers was added to wells of a black 96-well plate and data was collected using the GFP filter of a plate reader.

<u>Mass Spectrometry Analysis of CaM Proteins</u>

- Calcium calibration buffer kit, Invitrogen cat. no. C3008MP
- Chloroacetamide, Sigma cat. no. C0267
- TCEP, Sigma-Aldrich cat. no. C4706-2G
- Rappsilbers Stage tipping Paper (23), C-18 material: CDS Empore C18 Extraction Disks, Fisher cat. no. 13-110-016
- Formic acid for HPLC LiChropur, Sigma cat. no. 5438040100
- Trifluoroacetic acid (TFA), HPLC Grade, 99.5+%, Alfa Aesar, cat. no. AA446305Y
- Acetonitrile (ACN), Sigma-Aldrich cat. no. 271004-100ML
- Mass spectrometer: LC-MS: Orbitrap Fusion Lumos Tribrid (Thermo Fisher Scientific) and EASY-nLC™ 1200 System (Thermo Fisher Scientific)
- Triethylammonium bicarbonate buffer 1.0 M, pH 8.5±0.1, Sigma cat. no. T7408
- Ethanol for HPLC, Sigma cat. no. 459828
- Promega trypsin, cat no. V5111
- Methanol for HPLC, Sigma cat. No. 494291

StageTip Buffer A

- 5% ACN
- 0.1% TFA
- MQ water

StageTip Buffer B

- 0.1% TFA

- 80% ACN
- MQ water

Extraction solution

- 0.1% TFA, diluted in MQ water

Running the Gel

30 µg of wild-type CaM and N-terminus mutant CaM were each mixed with high Ca^{2+} calibration buffer to a final volume of 20 µl. A blank control consisting of CaM storage buffer and Ca^{2+} calibration buffer was also prepared. All samples were reduced using 1 mM final concentration of TCEP and alkylated using 2 mM final concentration of chloroacetamide (CAM) at 37C for 20 min on a shaker. They were then quenched using 1 mM final concentration of TCEP at 37C for 20 min on a shaker. Next, they were mixed with 5X gel loading buffer, boiled for five minutes, and loaded into a 10% gel (see "**Gel Electrophoresis**" above). The samples were run until the dye front reached the bottom of the gel. The gel was then rinsed and stained using Coomassie stain for one hour, and destained overnight.

In-gel Digestion Protocol

The next day, two bands from each lane were excised and cut into small cubes using a single-use scalpel; one band was comprised of the gel at ~18 kDa (where the major CaM band is located) and one was comprised of the gel between ~10 and 17 kDa, the area under the major band. The rest of the in-gel digestion was performed as previously described in (Lau et al., 2014).

Extraction of Peptides and StageTip Purification

StageTip extraction of peptides was performed as described previously in (23).

nanoLC-MS/MS Analyses

LC-MS analyses were performed as described previously with the following minor modifications (24). Peptide samples were separated on a EASY-nLC 1200 System (Thermo Fisher Scientific) using 20 cm long fused silica capillary columns (100 µm ID) packed with 3 µm 120 Å reversed phase C18 beads (Dr. Maisch, Ammerbuch, DE). The LC gradient was 90 min long with 5−35% B at 300 nL/min. LC solvent A was 0.1% (v/v) aq. acetic acid and LC solvent B was 20% 0.1% (v/v) acetic acid, 80% acetonitrile. MS data was collected with a Thermo Fisher Scientific Orbitrap Fusion Lumos Tribrid mass spectrometer. Data-dependent analysis was applied using Top15 selection with CID fragmentation

Computation of MS raw files

Data .raw files were analyzed by MaxQuant/Andromeda (25) version 1.5.2.8 using protein, peptide, and site FDRs of 0.01 and a score minimum of 40 for modified peptides, 0 for unmodified peptides; delta score minimum of 17 for modified peptides, 0 for unmodified peptides. MS/MS

spectra were searched against the UniProt human database (updated July 22nd, 2015). MaxQuant search parameters: Variable modifications included Oxidation (M) and Phospho (S/T/Y). Carbamidomethyl (C) was a fixed modification. Maximum missed cleavages was 2, enzyme was Trypsin/P and max. charge was 7. The MaxQuant "match between runs" feature was disabled. The initial search tolerance for FTMS scans was 20 ppm and 0.5 Da for ITMS MS/MS scans.

Semi-quantitative analysis of contaminants and CaM protein

The intensity of peptides annotated as CaM, keratin, or bacterial protein was summed up and their relative intensities were calculated by dividing them to the total peptide intensity in the samples.

Octet BioLayer Interferometry (BLI) measurement

- Octet Red 96 (ForteBio, Pall Life Sciences)
- Bovine Serum Albumin (BSA), Sigma-Aldrich cat. no. A3294-100G
- Calcium chloride, Sigma-Aldrich cat. no. 746495-1KG
- Tris-HCl, Sigma-Aldrich cat. no. T5941
- NaCl Sigma-Aldrich, # 746398-5KG

The binding of His-CaM to MLCK-Flag in the presence of Ca^{2+} was analyzed using the Octet Red 96 (ForteBio, Pall Life Sciences) following the manufacturer's procedures in duplicates. The reaction was carried out in black 96 well plates maintained at 30 °C. The reaction volume was 200 µL in each well. The Octet buffer contained 20 mM Tris-HCl, 200 mM NaCl, and 0.1% BSA, pH 8.0. The Association buffer contained 20 mM Tris-HCl, 200 mM NaCl, 1.5 mM Ca^{2+} and 0.1% BSA, pH 8.0. The Dissociation buffer contained 20 mM Tris-HCl, 200 mM NaCl, and 0.1% BSA, pH 8.0. The concentration of ligand, His-CaM^{WT}, His-CaM^{94A,130A}, or His-CaM$^{21A, 57A, 94A,130A}$, in the Octet buffer was 2 µM. The concentration of His-GST as the quench in Octet Buffer was 0.68 µM. The concentration of MLCK-Flag as the analyte in the Association buffer was 1.5 µM. Ni-NTA optical probes were loaded with His-CaM^{WT}, His-CaM^{94A,130A}, or His-CaM$^{21A, 57A, 94A,130A}$ as ligands for 110 seconds and quenched with His-GST for 80 seconds prior to binding analysis. While not loaded with ligand, the control probes were quenched with His-GST. The binding of the analyte, MLCK-Flag, to the optical probes was measured simultaneously using instrumental defaults for 236 seconds. The dissociation was measured for 287 seconds. There was no binding of the analyte to the unloaded probes. The data were analyzed by the Octet data analysis software. The association and dissociation curves were globally fit with a 1:1 ligand model. The data was plotted using Prism 7.

Data Reporting and Statistical Analysis

FR-CaM Binding Assay: For CaM^{WT} and $CaM^{21A,57A}$, each data point is presented as mean ± s.d. of 15 independent experiments. For $CaM^{94A,130A}$, each data point is presented as mean of ± s.d. of 8 independent experiments, and for $CaM^{21A,57A,94A,130A}$, each data point is presented as mean of ± s.d. of 3 independent experiments. For reporter-only data, each data point is presented as a mean ± s.d. of 17 independent experiments. Curve fits were computed using the Matlab (version R2020a) package doseResponse (https://www.mathworks.com/matlabcentral/fileexchange/33604-doseresponse).
Algebraic calculations involving the mathematical models were done in Mathematica (version 12.1).

Statistical Analysis: Statistical calculations were performed using Matlab. AUC was computed using the trapz built-in Matlab function.

DNA Sequences

CaM Sequences

Red highlighting: mutations

His-CaM^{WT} DNA Sequence (~19.8 kDa):

atgggcagcagccatcatcatcatcatcacagcagcggcctggtgccgcgcggcagccatagcgaaaacctctacttccaatcgat
ggctgaccagctgactgaggagcagattgcagagttcaaggaggccttctccctctttgacaaggatggagatggcactatcaccac
caaggagttggggacagtgatgagatccctgggacagaaccccactgaagcagagctgcaggatatgatcaatgaggtggatgca
gatgggaacgggaccattgacttcccggagttcctgaccatgatggccagaaagatgaaggacacagacagtgaggaggagatc
cgagaggcgttccgtgtctttgacaaggatgggaatggctacatcagcgccgcagagctgcgtcacgtaatgacgaacctggggga
gaagctgaccgatgaggaggtggatgagatgatcagggaggctgacatcgatggagatggccaggtcaattatgaagagtttgtac
agatgatgactgcaaagtga

His-$CaM^{21A,57A}$ DNA Sequence (~19.8 kDa):

atgggcagcagccatcatcatcatcatcacagcagcggcctggtgccgcgcggcagccatagcgaaaacctctacttccaatcgat
ggctgaccagctgactgaggagcagattgcagagttcaaggaggccttctccctctttgccaaggatggagatggcactatcaccac
caaggagttggggacagtgatgagatccctgggacagaaccccactgaagcagagctgcaggatatgatcaatgaggtggcagc
agatgggaacgggaccattgacttcccggagttcctgaccatgatggccagaaagatgaaggacacagacagtgaggaggagat
ccgagaggcgttccgtgtctttgacaaggatgggaatggctacatcagcgccgcagagctgcgtcacgtaatgacgaacctggggg

agaagctgaccgatgaggaggtggatgagatgatcagggaggctgacatcgatggagatggccaggtcaattatgaagagtttgta
cagatgatgactgcaaagtga

His-CaM^{94A,130A} DNA Sequence (~19.8 kDa):

atgggcagcagccatcatcatcatcatcacagcagcggcctggtgccgcgcggcagccatagcgaaaacctctacttccaatcgat
ggctgaccagctgactgaggagcagattgcagagttcaaggaggccttctccctctttgacaaggatggagatggcactatcaccac
caaggagttggggacagtgatgagatccctgggacagaaccccactgaagcagagctgcaggatatgatcaatgaggtggatgca
gatgggaacgggaccattgacttcccggagttcctgaccatgatggccagaaagatgaaggacacagacagtgaggaggagatc
cgagaggcgttccgtgtctttgccaaggatgggaatggctacatcagcgccgcagagctgcgtcacgtaatgacgaacctggggga
gaagctgaccgatgaggaggtggatgagatgatcagggaggctgccatcgatggagatggccaggtcaattatgaagagtttgtac
agatgatgactgcaaagtga

His-CaM^{21A,57A,94A,130A} DNA Sequence (~19.8 kDa):

atgggcagcagccatcatcatcatcatcacagcagcggcctggtgccgcgcggcagccatagcgaaaacctctacttccaatcgat
ggctgaccagctgactgaggagcagattgcagagttcaaggaggccttctccctctttgccaaggatggagatggcactatcaccac
caaggagttggggacagtgatgagatccctgggacagaaccccactgaagcagagctgcaggatatgatcaatgaggtggcagc
agatgggaacgggaccattgacttcccggagttcctgaccatgatggccagaaagatgaaggacacagacagtgaggaggagat
ccgagaggcgttccgtgtctttgccaaggatgggaatggctacatcagcgccgcagagctgcgtcacgtaatgacgaacctggggg
agaagctgaccgatgaggaggtggatgagatgatcagggaggctgccatcgatggagatggccaggtcaattatgaagagtttgta
cagatgatgactgcaaagtga

MLCK FR (~58.2 kDa)

Yellow highlighting: EYFP

Light grey highlighting: Calmodulin binding domain

Blue highlighting: ECFP

Dark grey highlighting: Flexible linker

Green highlighting: FLAG tag

FR DNA Sequence

Atggtgagcaagggcgaggagctgttcaccggggtggtgcccatcctggtcgagctggacggcgacgtaaacggccacaagttca
gcgtgtccggcgagggcgagggcgatgccacctacggcaagctgaccctgaagttcatctgcaccaccggcaagctgcccgtgcc
ctggcccaccctcgtgaccaccttcggctacggcctgatgtgcttcgcccgctaccccgaccacatgcgccagcacgacttcttcaagt
ccgccatgcccgaaggctacgtccaggagcgcaccatcttcttcaaggacgacggcaactacaagacccgcgccgaggtgaagtt
cgagggcgacaccctggtgaaccgcatcgagctgaagggcatcgacttcaaggaggacggcaacatcctggggcacaagctgg
agtacaactacaacagccacaacgtctatatcatggccgacaagcagaagaacggcatcaaggtgaacttcaagatccgccaca
acatcgaggacggcagcgtgcagctcgccgaccactaccagcagaacacccccatcggcaacggccccgtgctgctgcccgaca
accactacctgagctaccagtccgccctgagcaaagaccccaacgagaagcgcgatcacatggtcctgctggagttcgtgaccgcc

gccgggatcactctcggcatggacgagctgtacaagggtaccgccgctcgtcagaaatggcagaaaaccggacatgcggtgcgtg
cgattggccgtctggctgctaccggtagcaagggcgaggagctgttcaccggggtggtgcccatcctggtcgagctggacggcgac
gtaaacggccacaggttcagcgtgtccggcgagggcgagggcgatgccacctacggcaagctgaccctgaagttcatctgcacca
ccggcaagctgcccgtgccctggcccaccctcgtgaccaccctgacctggggcgtgcagtgcttcagccgctaccccgaccacatg
aagcagcacgacttcttcaagtccgccatgcccgaaggctacgtccaggagcgtaccatcttcttcaaggacgacggcaactacaa
gacccgcgccgaggtgaagttcgagggcgacaccctggtgaaccgcatcgagctgaagggcatcgacttcaaggaggacggca
acatcctggggcacaagctggagtacaactacatcagccacaacgtctatatcaccgccgacaagcagaagaacggcatcaagg
cccacttcaagatccgccacaacatcgaggacggcagcgtgcagctcgccgaccactaccagcagaacacccccatcggcgacg
gccccgtgctgctgcccgacaaccactacctgagcacccagtccgccctgagcaaagaccccaacgagaagcgcgatcacatgg
tcctgctggagttcgtgaccgccgccgggatcactctcggcatggacgagctgtacaagcccgggggtggatctggtggatctggtgg
atctatggattacaaggatgacgatgacaagtaa

ACKNOWLEDGEMENTS

We would like to thank Dr. Ning Zheng and Dr. Haibin Mao for their help with protein purification, Dr. Martin Golkowski for his help with mass spectrometry, Dr. Anthony Persechini for providing the MLCK FR construct, and Dr. Zenon Grabarek and Dr. John Biddle for comments on the manuscript. The authors are also grateful to UW's elevator maintenance team for rescuing MJSM (and several liters of induced bacteria) from a stalled elevator during the writing of this manuscript.

AUTHOR CONTRIBUTIONS

MJSM, JPD, and YS designed the experiments and wrote the manuscript. MJSM, HE, and YS performed cloning, binding assays, and other biochemical experiments. DVR performed BLI experiments. MJSM, JPD, and YS analyzed the data. JPD developed the mathematical models.

FUNDING AND ADDITIONAL INFORMATION

MJSM was supported by NIH grant T32GM007750; JPD was supported by a Neukom Fellowship and a Harvard Data Science Fellowship.

CONFLICT OF INTEREST

The authors declare no conflicts of interest.

ABBREVIATIONS AND NOMENCLATURE

CaM^{WT} – wild-type calmodulin

$CaM^{21A,57A}$ – calmodulin with N-terminus D21A and D57A mutations

$CaM^{94A,130A}$ – calmodulin with C-terminus D94A and D130A mutations

$CaM^{21A,57A,94A,130A}$ – calmodulin with N-terminus D21A and D57A mutations, and C-terminus D94A and D130A mutations

FR – FRET Reporter

FRET – fluorescence resonance energy transfer

HEK 293T – human embryonic kidney 293T cells

MLCK – myosin light chain kinase

STR analysis – short tandem repeat analysis

REFERENCES

1. Babu, Y. S., Sack, J. S., Greenhough, T. J., Bugg, C. E., Means, A. R., and Cook, W. J. (1985) Three-dimensional structure of calmodulin. *Nature* **315**, 37-40
2. Webb, R. C. (2003) Smooth muscle contraction and relaxation. *Adv Physiol Educ* **27**, 201-206
3. Swulius, M. T., and Waxham, M. N. (2008) Ca(2+)/calmodulin-dependent protein kinases. *Cell Mol Life Sci* **65**, 2637-2657
4. Xia, Z., and Storm, D. R. (2005) The role of calmodulin as a signal integrator for synaptic plasticity. *Nat Rev Neurosci* **6**, 267-276
5. Park, H. Y., Kim, S. A., Korlach, J., Rhoades, E., Kwok, L. W., Zipfel, W. R., Waxham, M. N., Webb, W. W., and Pollack, L. (2008) Conformational changes of calmodulin upon Ca2+ binding studied with a microfluidic mixer. *Proc Natl Acad Sci U S A* **105**, 542-547
6. Adelstein, R. S., and Sellers, J. R. (1987) Effects of calcium on vascular smooth muscle contraction. *Am J Cardiol* **59**, 4B-10B
7. Hong, F., Haldeman, B. D., Jackson, D., Carter, M., Baker, J. E., and Cremo, C. R. (2011) Biochemistry of smooth muscle myosin light chain kinase. *Arch Biochem Biophys* **510**, 135-146
8. Brown, S. E., Martin, S. R., and Bayley, P. M. (1997) Kinetic control of the dissociation pathway of calmodulin-peptide complexes. *J Biol Chem* **272**, 3389-3397
9. Fajmut, A., Brumen, M., and Schuster, S. (2005) Theoretical model of the interactions between Ca2+, calmodulin and myosin light chain kinase. *FEBS Lett* **579**, 4361-4366
10. Fajmut, A., Jagodic, M., and Brumen, M. (2005) Mathematical modeling of the myosin light chain kinase activation. *J Chem Inf Model* **45**, 1605-1609
11. Kato, S., Osa, T., and Ogasawara, T. (1984) Kinetic model for isometric contraction in smooth muscle on the basis of myosin phosphorylation hypothesis. *Biophys J* **46**, 35-44
12. Dexter, J. P., Biddle, J. W., and Gunawardena, J. (2018) Model discrimination for Ca(2+) -dependent regulation of myosin light chain kinase in smooth muscle contraction. *FEBS Lett* **592**, 2811-2821
13. Raina, H., Zacharia, J., Li, M., and Wier, W. G. (2009) Activation by Ca2+/calmodulin of an exogenous myosin light chain kinase in mouse arteries. *J Physiol* **587**, 2599-2612
14. Wier, W. G., Rizzo, M. A., Raina, H., and Zacharia, J. (2008) A technique for simultaneous measurement of Ca2+, FRET fluorescence and force in intact mouse small arteries. *J Physiol* **586**, 2437-2443
15. Wang, Y., Chen, L., Wier, W. G., and Zhang, J. (2013) Intravital Forster resonance energy transfer imaging reveals elevated [Ca2+]i and enhanced sympathetic tone in femoral arteries of angiotensin II-infused hypertensive biosensor mice. *J Physiol* **591**, 5321-5336
16. Mauban, J. R., Fairfax, S. T., Rizzo, M. A., Zhang, J., and Wier, W. G. (2014) A method for noninvasive longitudinal measurements of [Ca2+] in arterioles of hypertensive optical biosensor mice. *Am J Physiol Heart Circ Physiol* **307**, H173-181
17. Zhang, J., Wang, Y., Chen, L., Wier, W. G., and Blaustein, M. P. (2019) Na(+)/Ca(2+) exchanger overexpression in smooth muscle augments cytosolic Ca(2+) in femoral arteries of living mice. *Am J Physiol Heart Circ Physiol* **316**, H298-H310
18. Calizo, R. C., Bell, M. K., Ron, A., Hu, M., Bhattacharya, S., Wong, N. J., Janssen, W. G. M., Perumal, G., Pederson, P., Scarlata, S., Hone, J., Azeloglu, E. U., Rangamani, P., and Iyengar, R. (2020) Cell shape regulates subcellular organelle location to control early Ca(2+) signal dynamics in vascular smooth muscle cells. *Sci Rep* **10**, 17866

19. Geguchadze, R., Zhi, G., Lau, K. S., Isotani, E., Persechini, A., Kamm, K. E., and Stull, J. T. (2004) Quantitative measurements of Ca(2+)/calmodulin binding and activation of myosin light chain kinase in cells. *FEBS Lett* **557**, 121-124
20. Wallace, R. W., Tallant, E. A., Dockter, M. E., and Cheung, W. Y. (1982) Calcium binding domains of calmodulin. Sequence of fill as determined with terbium luminescence. *J Biol Chem* **257**, 1845-1854
21. Chang, A. N., Mahajan, P., Knapp, S., Barton, H., Sweeney, H. L., Kamm, K. E., and Stull, J. T. (2016) Cardiac myosin light chain is phosphorylated by Ca2+/calmodulin-dependent and -independent kinase activities. *Proc Natl Acad Sci U S A* **113**, E3824-3833
22. Aoki, H., Sadoshima, J., and Izumo, S. (2000) Myosin light chain kinase mediates sarcomere organization during cardiac hypertrophy in vitro. *Nat Med* **6**, 183-188
23. Rappsilber, J., Mann, M., and Ishihama, Y. (2007) Protocol for micro-purification, enrichment, pre-fractionation and storage of peptides for proteomics using StageTips. *Nat Protoc* **2**, 1896-1906
24. Golkowski, M., Lau, H. T., Chan, M., Kenerson, H., Vidadala, V. N., Shoemaker, A., Maly, D. J., Yeung, R. S., Gujral, T. S., and Ong, S. E. (2020) Pharmacoproteomics Identifies Kinase Pathways that Drive the Epithelial-Mesenchymal Transition and Drug Resistance in Hepatocellular Carcinoma. *Cell Syst* **11**, 196-207 e197
25. Cox, J., Neuhauser, N., Michalski, A., Scheltema, R. A., Olsen, J. V., and Mann, M. (2011) Andromeda: a peptide search engine integrated into the MaxQuant environment. *J Proteome Res* **10**, 1794-1805

FIGURE 1

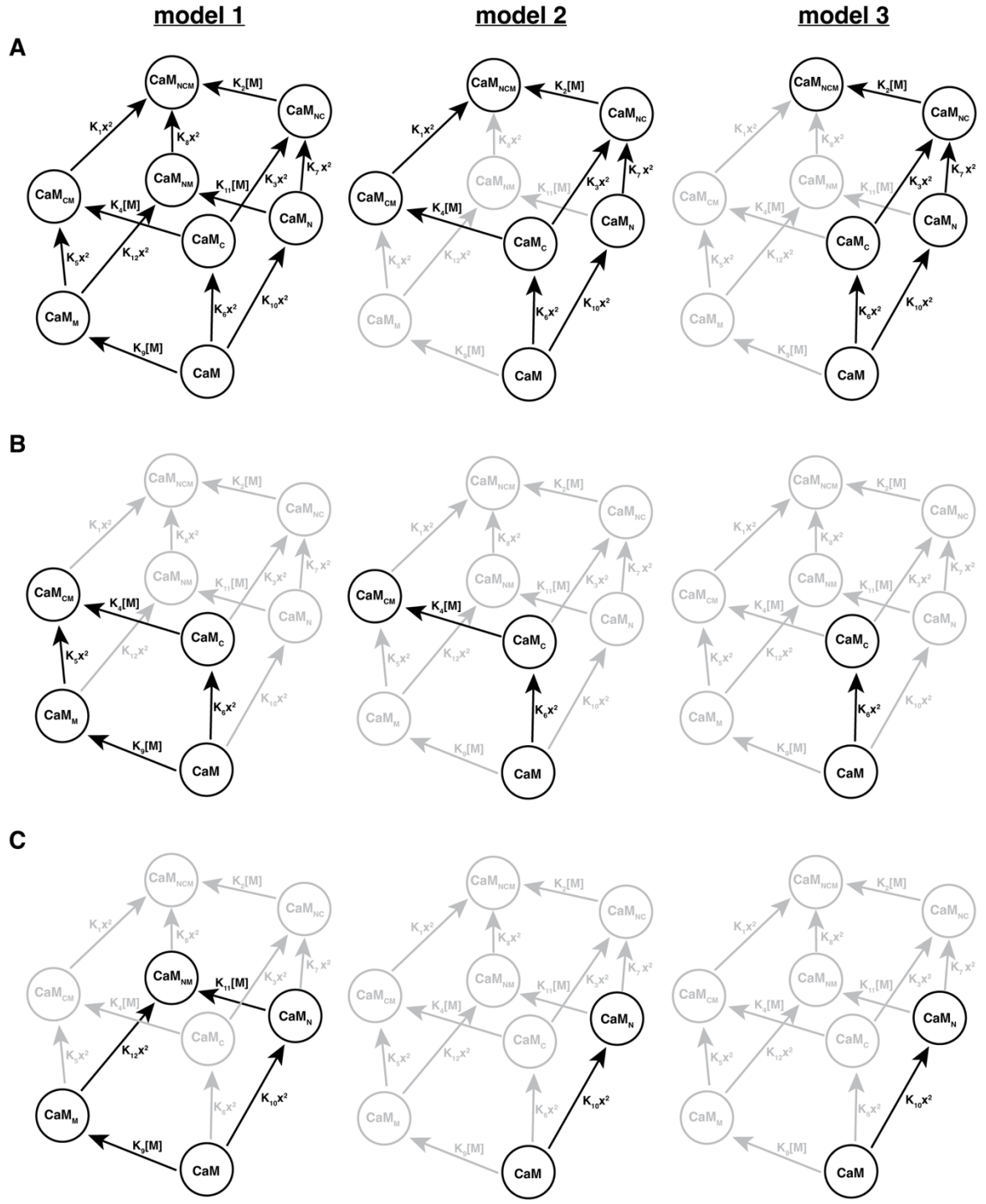

Figure 1: Network diagrams for the binding of Ca^{2+} and MLCK to CaM. Model 1 is the unordered model proposed by Brown *et al*. (8) and Fajmut, Brumen *et al*. (9); models 2 and 3 correspond to the partially and fully ordered models of Fajmut, Jagodic *et al*. (10) and Kato *et al*. (11), respectively. **(A)** shows the networks for CaM^{WT}, **(B)** for $CaM^{21A,57A}$, and **(C)** for $CaM^{94A,130A}$ Models 2 and 3 are truncations of Model 1; omitted edges and vertices are shown in gray. In each network *x* denotes $[Ca^{2+}]$, and *M* denotes MLCK. The subscripts N and C indicate Ca^{2+} binding at

the N-terminal and C-terminal EF hands of CaM, respectively, and the subscript M indicates MLCK binding. The figure is adapted from Dexter *et al*. (12).

FIGURE 2

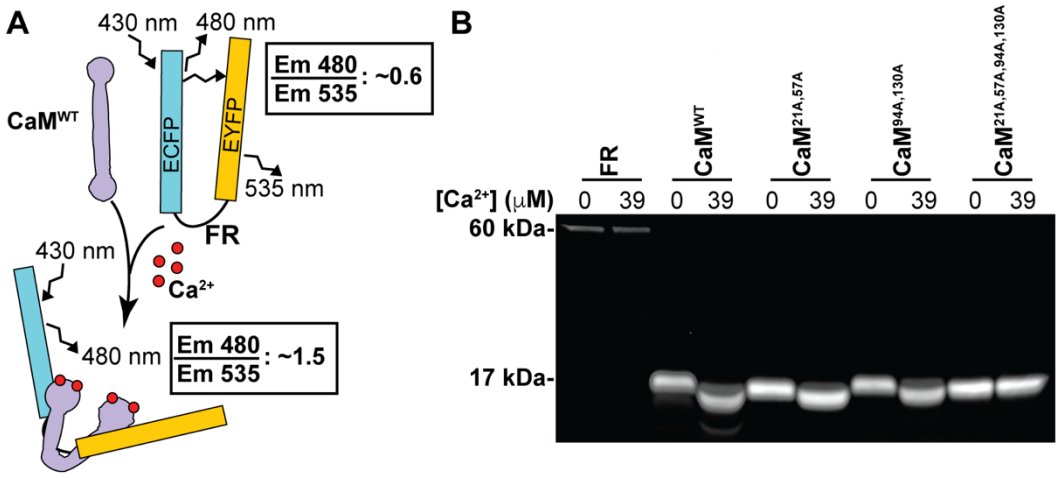

Figure 2: MLCK-based FRET assay reports MCLK-CaM binding. (A) Schematic showing assay principle. In the presence of Ca^{2+}, CaM binds to the CaM-binding domain of the FR, leading to a decrease in FRET and reduced emission at 535 nm. **(B)** Representative gel image of purified FR and CaM proteins visualized with SYPRO™ Ruby protein gel stain following SDS-PAGE. Samples were incubated in buffers containing either 0 μM Ca^{2+} or 39 μM free Ca^{2+} before SDS-PAGE. 8 μg of each CaM protein and 800 ng of FR was loaded.

FIGURE 3

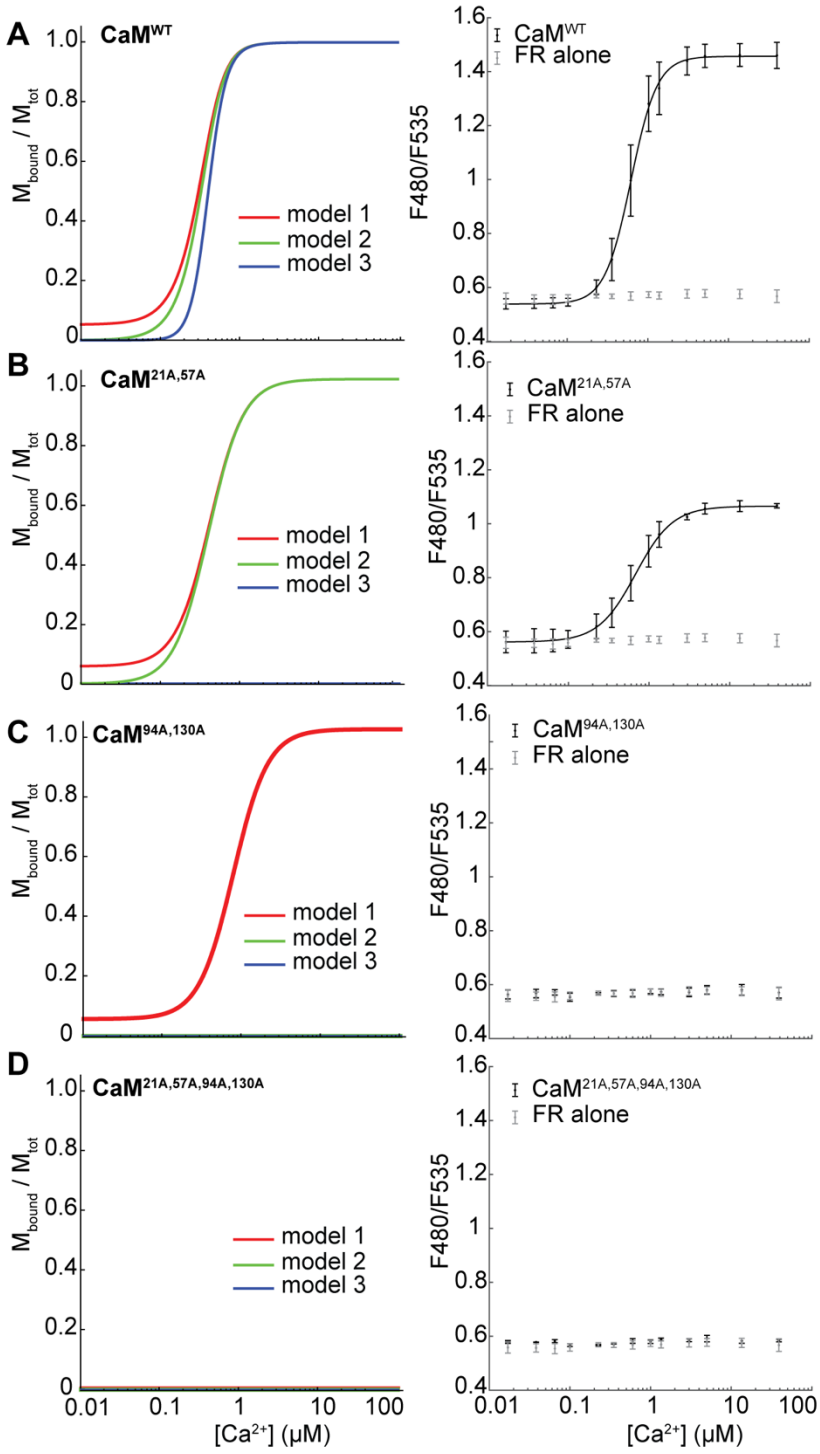

Figure 3: Predictions of mathematical models of MLCK binding and FRET measurements in the presence of excess CaM relative to FR. Theoretical (left) and experimental binding curves (right) for **(A)** CaM^{WT}, **(B)** $CaM^{21A,57A}$, **(C)** $CaM^{94A,130A}$, and **(D)** $CaM^{21A,57A,94A,130A}$. The theoretical curves were calculated assuming [CaM] = 0.713 μM and [MLCK] = 0.0237 μM (the concentrations used in the main experiments) and the reference parameter values from Fajmut,

Brumen *et al*. (9). For the experiments, FR was incubated either alone, or with a 30-fold excess of CaM^{WT}, $CaM^{21A,57A}$, $CaM^{94A,130A}$, $CaM^{21A,57A,94A,130A}$, in the presence of indicated [Ca^{2+}] in 96-well plates. Emission at 480 nm and 535 nm was measured after excitation at 430 nm using a plate reader. The [Ex430, Em480] fluorescence intensity was then divided by the [Ex430, Em535] intensity to yield an emission ratio, which is plotted. Shown are mean ± standard deviation of 17 replicates for FR only, 15 replicates for CaM^{WT}, 15 replicates for $CaM^{21A,57A}$, 8 replicates for $CaM^{94A,130A}$, and 3 replicates for $CaM^{21A,57A,94A,130A}$.

FIGURE 4

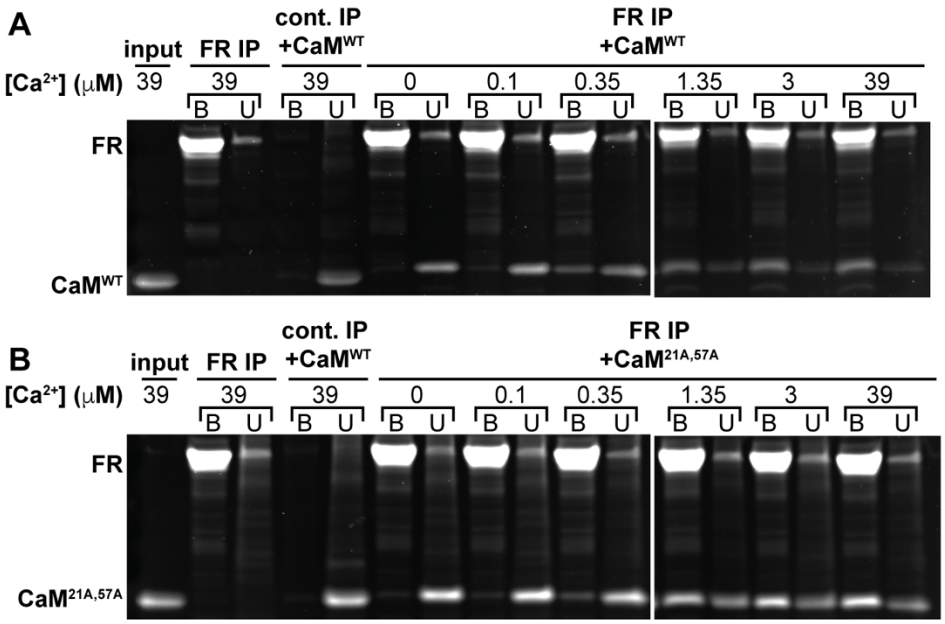

Figure 4: Purified CaM^{WT} and $CaM^{21A,57A}$ show Ca^{2+}-dependent interaction with FR. Representative images showing *in vitro* binding between immunoprecipitated FR and **(A)** CaM^{WT} or **(B)** $CaM^{21A,57A}$ in buffers with the indicated free [Ca^{2+}]. Unbound and bound fractions were analyzed by SDS-PAGE followed by SYPRO™ Ruby protein gel stain. FR without CaM addition and an immunoprecipitation from non-transfected HEK 293T cells serve as controls. The input lane shows the purified CaM^{WT} or $CaM^{21A,57A}$ added to the *in vitro* binding assay.

FIGURE 5

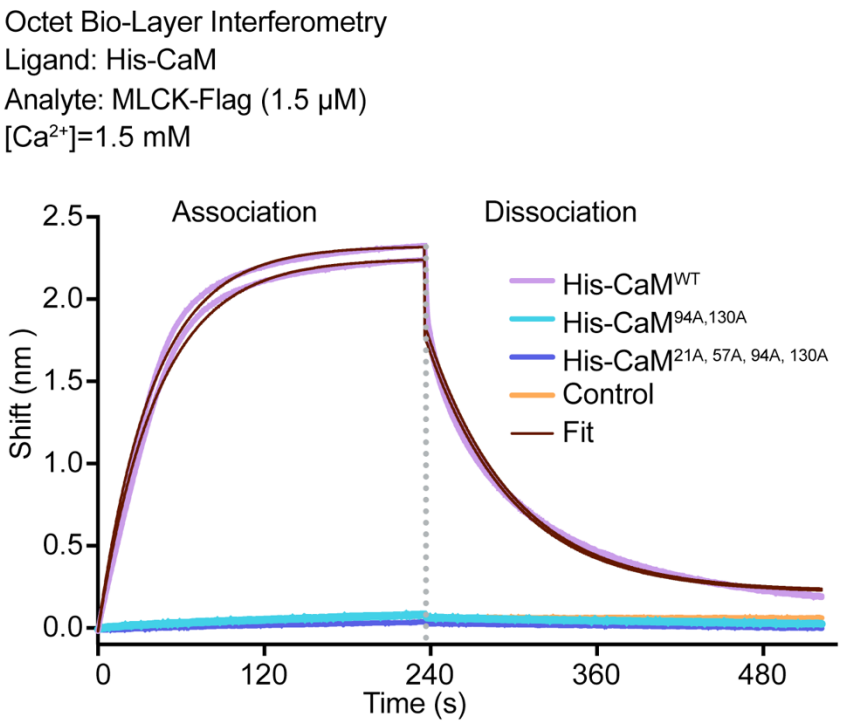

Figure 5: Bio-Layer Interferometry (BLI) binding assays do not show FR-CaM^{94A,130A} or FR-CaM^{21A,57A,94A,130A} binding. BLI was performed using purified HIS-tagged calmodulin (CaM^{WT}, CaM^{94A,130A}, or CaM^{21A,57A,94A,130A}) and FLAG-tagged FR. Calmodulin served as the ligand and was immobilized to a Ni-NTA biosensor, while the FR served as the analyte. Two replicates of each condition are shown.

TABLE 1

		model 1	model 2	model 3	observed
zero Ca^{2+}					
	CaM^{WT}	**B**	NB	NB	NB
	$CaM^{21A,57A}$	**B**	NB	NB	NB
	$CaM^{94A,130A}$	**B**	NB	NB	NB
high Ca^{2+}					
	CaM^{WT}	B	B	B	B
	$CaM^{21A,57A}$	B	B	**NB**	B
	$CaM^{94A,130A}$	**B**	NB	NB	NB

Table 1: Summary of model discrimination results for CaM and MLCK binding. B denotes binding, NB denotes no binding. Bolded entries indicate experimentally falsified predictions.

SUPPLEMENTARY FIGURE 1

A

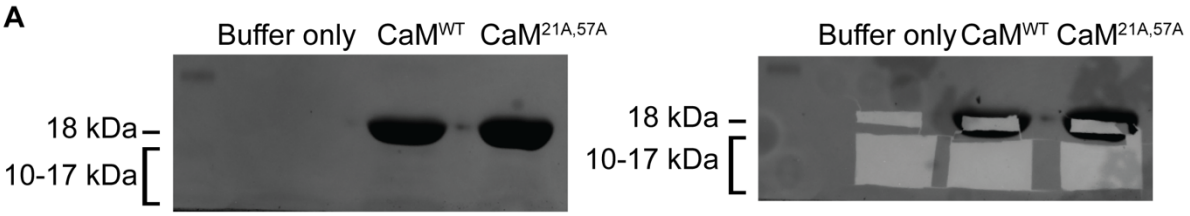

B

	% CaM intensity			% Keratin, E.coli proteins		
Molecular Weight	Buffer only	CaM^{WT}	$CaM^{21A,57A}$	Buffer only	CaM^{WT}	$CaM^{21A,57A}$
18 kDa	17%	96%	99%	34%	0%	0%
10-17 kDa	53%	91%	66%	11%	3%	15%
Lane total	51%	96%	96%	13%	1%	2%

Supplementary Figure 1: Mass spectrometry analysis of purified calmodulin proteins. Semi-quantitative mass spectrometry was performed to assess the purity of purified CaM^{WT} and $CaM^{21A,57A}$ proteins; a "loading buffer only" lane was used as a control. **(A)** Following SDS-PAGE, the gel was Coomassie stained, and bands of interest were excised and analyzed by mass spectrometry. **(B**) The identified peptides were categorized as CaM or a contaminating protein (keratin or *E. coli* protein) using their annotations. Finally, the percent abundance of either CaM or contaminants in each band was determined using their intensity in mass spectrometry data

SUPPLEMENTARY FIGURE 2

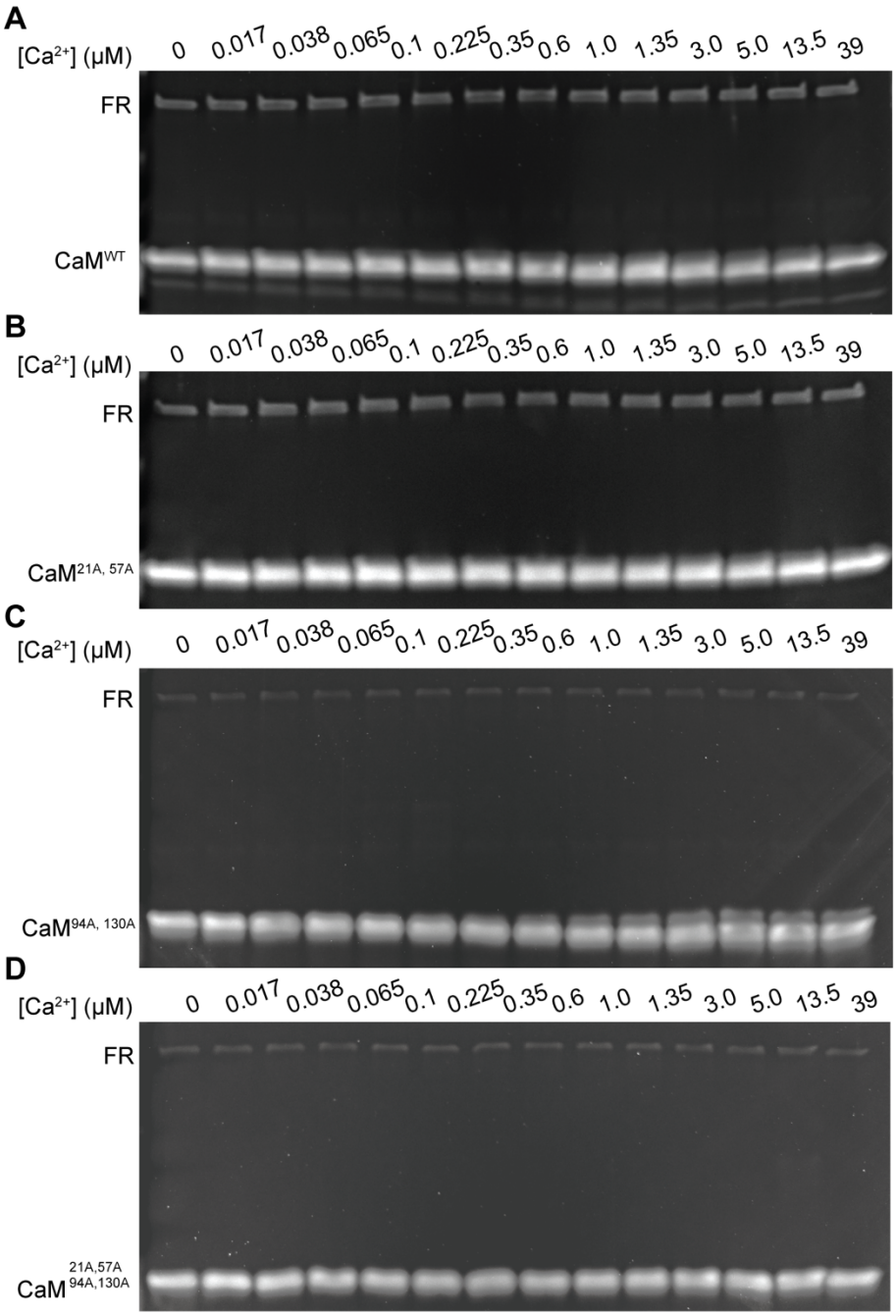

Supplementary Figure 2: Purified FR and CaM used in data collection. A portion of each sample for fluorescent detection of FR-CaM binding was recovered from the wells. SDS-PAGE and SYPRO™ Ruby staining confirmed the presence of excess CaM compared to FR in the assay for **(A)** CaM^{WT} and FR, **(B)** $CaM^{21A,57A}$ and FR, **(C)** $CaM^{94A,130A}$ and FR, and **(D)** $CaM^{21A,57A,94A,130A}$

SUPPLEMENTARY FIGURE 3

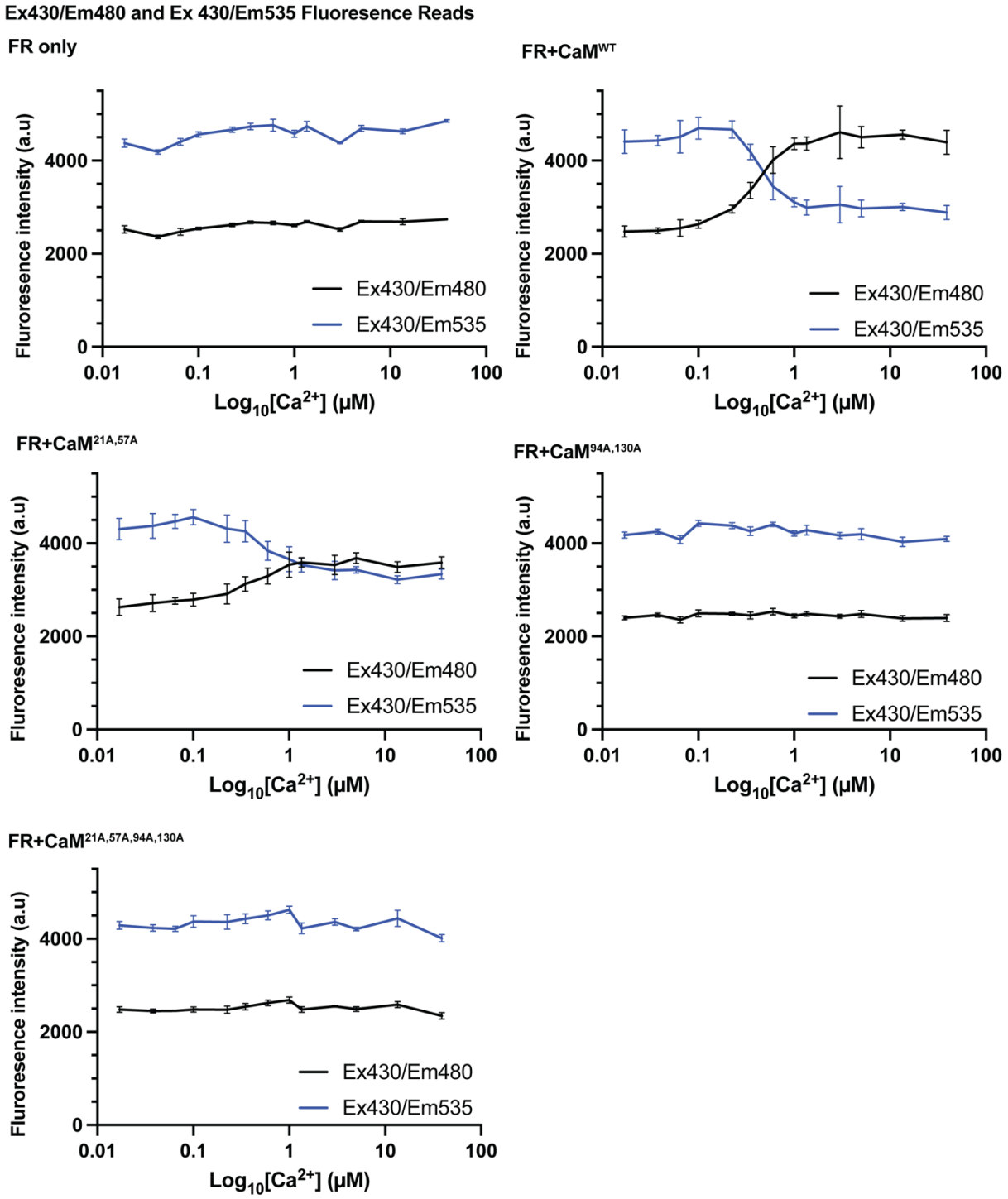

Supplementary Figure 3: Raw fluorescence intensities of FR-CaM binding assay. For each of the indicated CaM-FR combinations, 673 nM CaM and 22.9 nM FR were combined in 150 µl

of Ca^{2+} buffer (14 conditions between 0 μM and 39 μM). Fluorescence intensity of [Ex430, Em480], followed by intensity of [Ex430, Em535], was measured using a plate reader. Shown are mean ± standard deviation of raw data from at least 5 replicates for CaM^{WT}, $CaM^{21A,57A}$, and $CaM^{94A,130A}$, and 3 replicates for $CaM^{21A,57A,94A,130A}$ and FR only. **Fig. 3** shows the full dataset following analysis.

SUPPLEMENTARY FIGURE 4

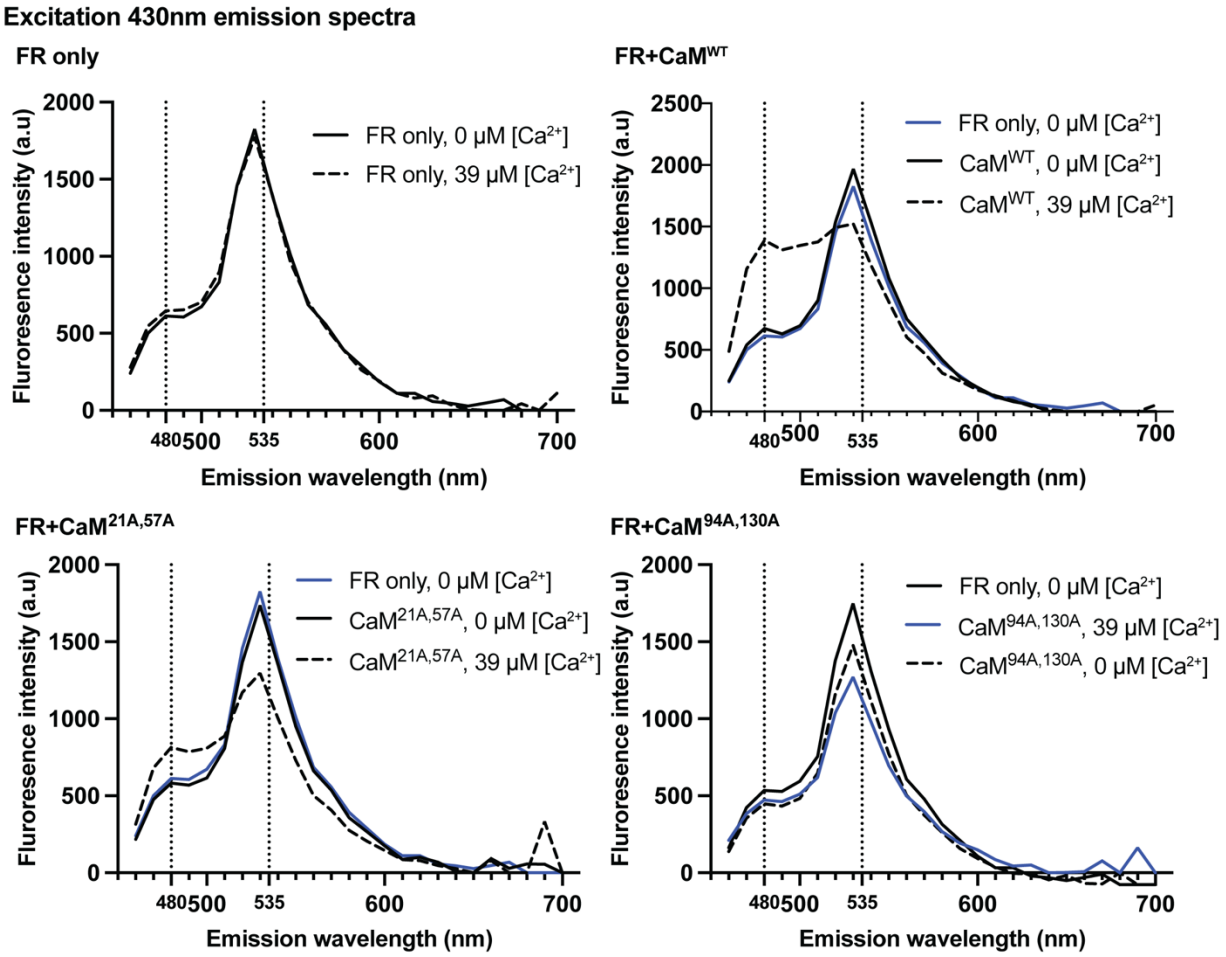

Supplementary Figure 4. Emission spectra of FR at Ex430. The emission spectra (460 nm - 700 nm, 10 nm steps) of FR alone or with calmodulin (CaM^{WT}, $CaM^{21A,57A}$, or $CaM^{94A,130A}$) was measured at either 0 or 39 μM [Ca^{2+}]. Dotted lines indicate the Em480 and Em535 wavelengths, which were used in FRET-based FR-CaM binding assays. One representative read for each condition is shown. FR-only spectra are included in the CaM graphs as a reference.

SUPPLEMENTARY FIGURE 5

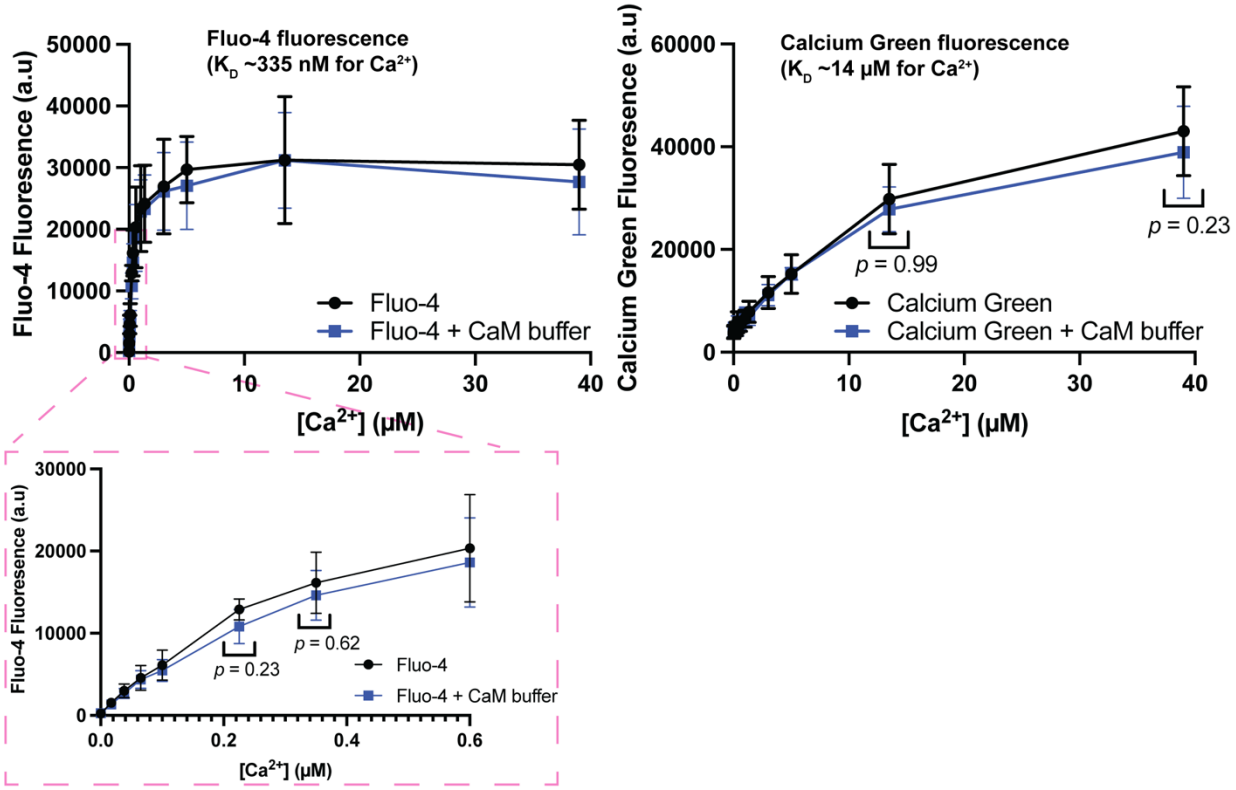

Supplementary Figure 5. Buffer addition to FR-CaM binding assay does not change assay free [Ca^{2+}]. Ca^{2+} indicator dyes Fluo-4 or Calcium Green were added to the 14-buffer series of the FR-CaM binding assay; data was collected using a plate reader with a GFP filter. The same buffer/Ca^{2+} indicator dye combinations were then assayed following the addition of a "dummy buffer" composed of the buffer in which all CaM proteins were stored. The area of interest (magnified region in red dotted line) highlights the data corresponding to [Ca^{2+}] most relevant to Fluo-4, which has K_D~335 nM. Calcium Green has K_D~14 μM. Mean ± standard deviation of four replicates for each condition are shown. *P* values were calculated using a two-tailed Mann-Whitney *U* test.

SUPPLEMENTARY FIGURE 6

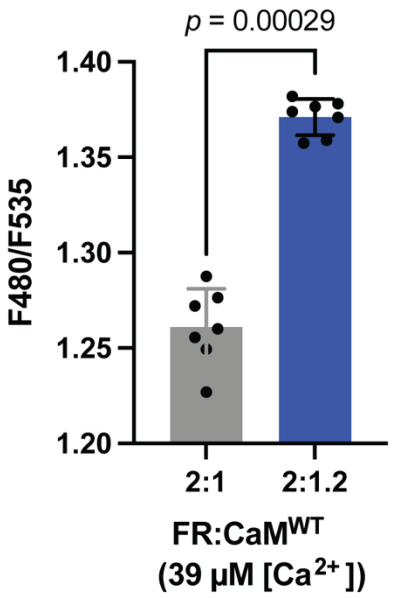

Supplementary Figure 6: FR-CaM binding assay is sensitive enough to detect a 9% increase in CaM-FR binding. A modified version of the FR-CaM binding assay using a FR:CaM^{WT} ratio of either 2:1 or 2:1.2 (22.9 nM FR and 11.45 nM or 13.75 nM CaM) in high [Ca^{2+}] was performed. The F480/F535 ratios increased significantly between conditions (p = 0.00029 by a one-tailed Mann-Whitney U test), and the percent difference (8.7%) matched the change predicted theoretically assuming Model 2 and the reference parameter values from Fajmut, Brumen *et al*. (9) (46.2% to 54.7%). Mean ± standard deviation of 7 replicates for each condition are shown.

SUPPLEMENTARY FIGURE 7

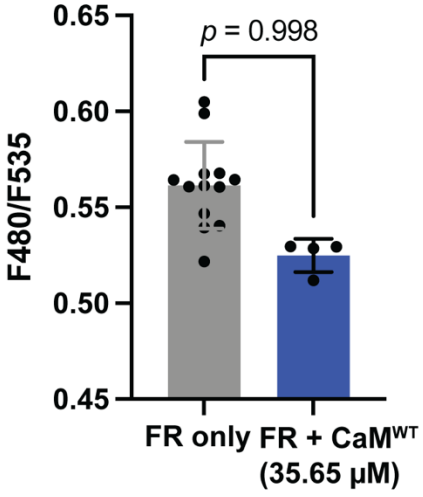

Supplementary Figure 7: CaM^{WT} does not bind to FR in the absence of Ca^{2+} even at high concentrations. To test the robustness of our observation of no binding in zero [Ca^{2+}], we repeated the binding assay with 35.65 μM CaM^{WT}, for which Model 1 predicts 21.7% binding even if previous estimates of a key parameter value are incorrect by an order of magnitude. CaM^{WT} was concentrated to 66.6 μg/μl so that the volume of protein solution used was comparable to previous assays. As in the original assay, the F480/F535 ratio was not higher than baseline (p = 0.998 by a one-tailed Mann-Whitney U test). Mean ± standard deviation of 13 replicates for FR only read and 4 replicates for FR+ CaM^{WT} reads are shown.

SUPPLEMENTRAY FIGURE 8

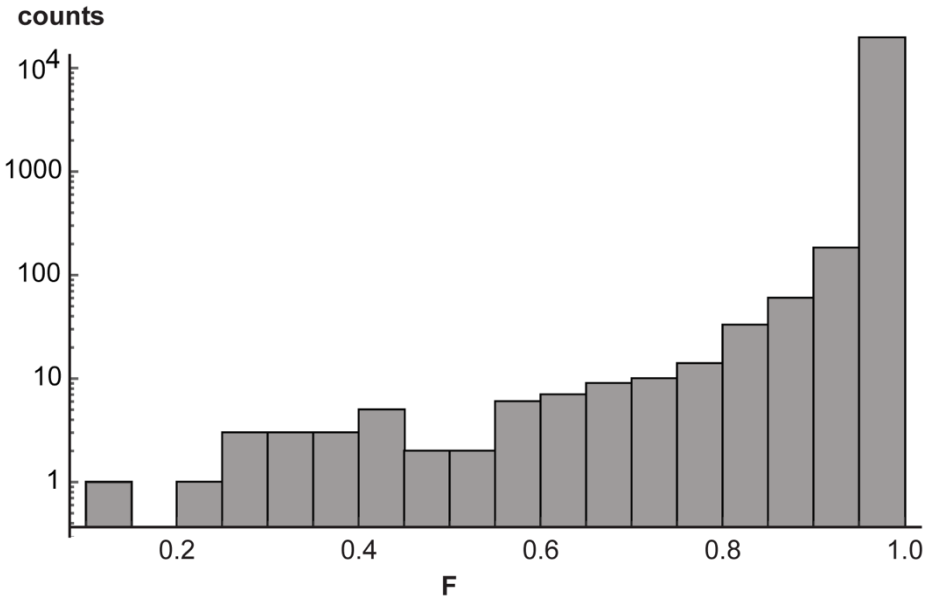

Supplementary Figure 8. Histogram from sensitivity analysis of model of CaM^{21A,57A}. The histogram shows the distribution of predicted binding fractions for 200,000 combinations of K_4 and K_6 chosen at random from the interval [0.1v, 10v], where v is the reference value from Fajmut, Brumen *et al*. (9).